Gem News International

Contributing Editors
Emmanuel Fritsch, *University of Nantes, CNRS, Team 6502, Institut des Matériaux Jean Rouxel (IMN), Nantes, France* (fritsch@cnrs-imn.fr)
Gagan Choudhary, *Gem Testing Laboratory, Jaipur, India* (gagan@gjepcindia.com)
Christopher M. Breeding, *GIA, Carlsbad* (christopher.breeding@gia.edu)

COLORED STONES AND ORGANIC MATERIALS

Unique metal sulfide inclusion in "Bing Piao" red agate from Liangshan, China. Over the past decade, with the discovery of "Nanhong" agate ore deposits in Sichuan Province, a significant amount of this material has been mined in Meigu County, located in the northeast of Liangshan Yi Autonomous Prefecture. Commercial gem mines in Meigu County are located in three main areas, including Jiu Kou, Wa Xi, and Lian He. Field observations show that the ore body is found either in the interlayer fissures and cavities of Permian Emeishan basalt crystallized from siliceous hydrothermal fluid or as conglomerates of the Permian Leping Formation.

Previous reports found that "Nanhong" agate is colored by natural hematite inclusions. Moreover, these agates are divided into five major categories, including "Bing Piao" (a Chinese term that refers to their inclusions "floating on ice"). This type of agate (see figure 1, left) is colorless and contains red hematite particles distributed in attractive patterns.

Recently, a special type of "Bing Piao" red agate called "black grass" agate by merchants appeared in the market at Liangshan. A bead of this material (figure 1, right) was obtained for examination at the National Gold-Silver Gem & Jewelry Quality Supervision & Inspection Center (Sichuan).

Gemological properties of the semitransparent bead, including its RI of 1.54 and hydrostatic SG of 2.65, suggested agate; this was confirmed by FTIR spectroscopy. Magnification revealed tiny red inclusions that were identified as hematite by Raman spectra (peaks at 225, 244, 291, 410, 610, and 1320 cm^{-1}) using a 785 nm laser. In addition to these attractive red forms made of hematite, the bead hosted many unusual black mineral particles displaying various shapes such as blades, planar clusters, and the like (figure 2). When viewed with reflected light, microscopic observations of their opaque, anhedral form and metallic luster suggested the particles were likely an iron sulfide. A Raman spectrum obtained from a surface-reaching black particle showed two major peaks at 342 and 377 cm^{-1}, matching well with pyrite, according to the RRUFF database (reference spectrum R100166), as shown in figure 3.

To obtain confirmation, the bead was polished down to a plate to perform chemical analysis and phase identification of the black particles using a scanning electron microscope in combination with an energy-dispersive

Figure 1. The cabochon on the left is a normal "Bing Piao" red agate measuring 12.50 × 19.60 × 10.11 mm. The bead on the right, approximately 11.80 mm in diameter, is a special type of "Bing Piao" red agate. Photo by Su Xu.

Editors' note: Interested contributors should send information and illustrations to Stuart Overlin at soverlin@gia.edu or GIA, The Robert Mouawad Campus, 5345 Armada Drive, Carlsbad, CA 92008.

Gems & Gemology, Vol. 57, No. 2, pp. 166–184.

© 2021 Gemological Institute of America

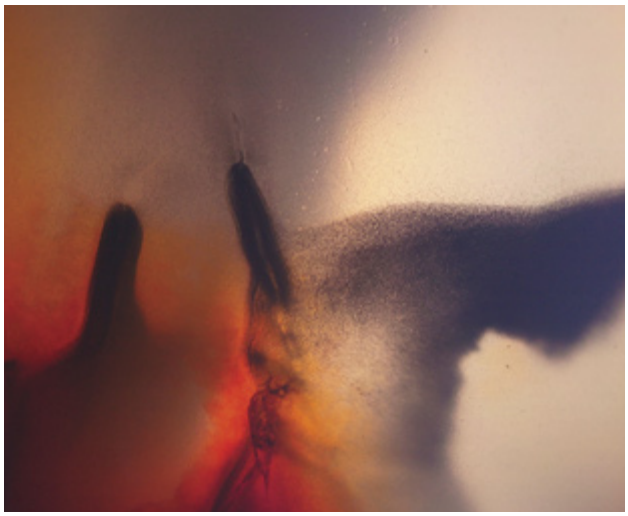

Figure 2. These antennae-like inclusions consist of dot-like black minerals, coupled with red inclusions. Photomicrograph by Xiaoping Shi; field of view 9.00 mm.

spectrometer (SEM-EDS) equipped with an electron backscatter diffraction (EBSD) detector. Qualitative analysis revealed the expected major elements of Fe, As, and S, along with minor Si, likely from the agate host. This was consistent with pyrite composition. The EBSD analyses indicated a cubic structure, and a search of the NIST Structural Database using Aztec software revealed a match for pyrite (FeS_2).

Figure 3. The black particle was identified as pyrite based on comparison with Raman reference spectra from the RRUFF database. Spectra are offset vertically for clarity.

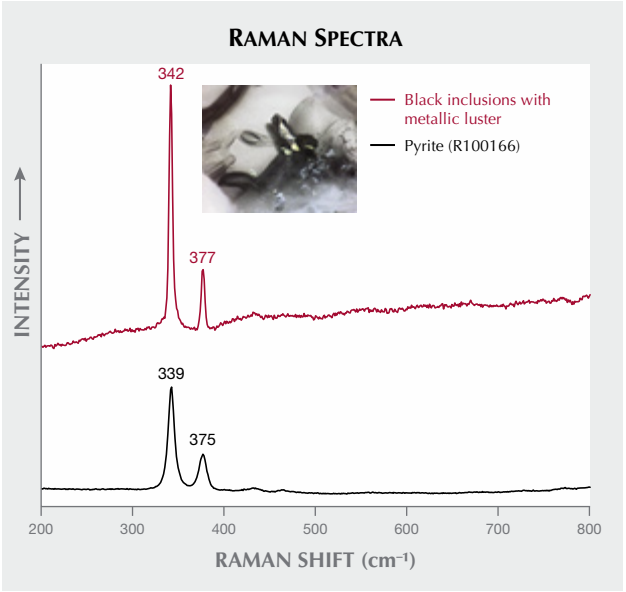

Except for Liangshan, such distinctive black minerals of various forms have not been found in other "Bing Piao" red agate deposits. The pyrite particles, as inclusions that are unique to "Bing Piao" red agate from Liangshan, may therefore be considered reliable indicators of origin. Further gemological studies on these inclusions are required to construct the database for origin determination.

Su Xu and Dapeng Chen
National Gold-Silver Gem & Jewelry Quality Supervision & Inspection Center (Sichuan)
Xiaoping Shi
Sichuan Provincial Coal Design & Research Institute

Natural freshwater pearls from Europe: Russia, Scotland, and Germany. The Carlsbad laboratory received eight European freshwater (FW) pearls from coauthor ES for gemological and chemical characterization (figure 4). Although the exact locations and times of discovery were not recorded, all the samples were obtained directly by ES from reputable sources in each country. The first three samples are of Russian origin and were obtained by Russian fisheries biologist Valery Ziuganov during his studies of the Varzuga River, Kola Peninsula, in the 1990s (E. Strack, "European freshwater pearls: Part 1–Russia," *Journal of Gemmology*, Vol. 34, No. 7, 2015, pp. 580–593; E. Strack, "Freshwater pearls from Russia," *Margaritologia*

Figure 4. The eight European natural freshwater pearls reportedly produced by Margaritifera margaritifera *mussel species, collected from freshwater sources in Russia, Scotland, and Germany. Photo by Diego Sanchez.*

TABLE 1. Internal structures of eight European freshwater pearls revealed by RTX and μ-CT analyses.

Sample number, origin, and weight	Macro image	RTX image	μ-CT image
No. 1, Russia 1.27 ct		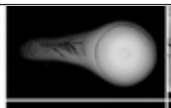	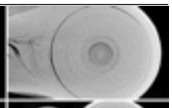
No. 2, Russia 1.83 ct		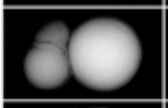	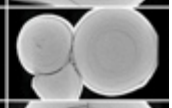
No. 3, Russia 2.68 ct		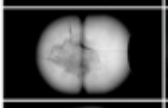	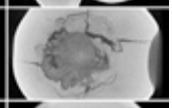
No. 4, Scotland 0.70 ct		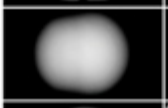	
No. 5, Scotland 1.52 ct		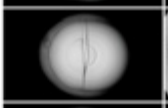	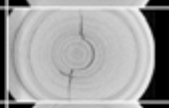
No. 6, Germany 0.94 ct		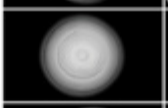	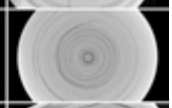
No. 7, Germany 1.61 ct		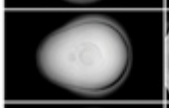	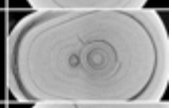
No. 8, Germany 2.11 ct		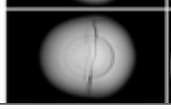	

newsletter, No. 11, 2018). Two samples from Scottish rivers were provided in 2004 by Cairncross Jewellers, the only company allowed to buy pearls from the fishers in Perth, Scotland. The last three are from Lüneburg Heath in northern Germany and were supplied around 1997 by a local family that had collected and fished for pearls over the decades. European FW natural pearls have reportedly been produced for centuries from mussels belonging to the *Margaritifera margaritifera* species, which has been referred to as the "freshwater pearl mussel" (E. Strack, *Pearls*, Rühle-Diebener-Verlag, Stuttgart, Germany, 2006). Today, most natural FW pearls produced in North America and cultured FW pearls from Asia form in various mussel species within the *Unionidae* family. Both families are member of the Unionoidea superfamily.

The samples exhibited two different surface structures: nacreous and non-nacreous. Upon examination with a loupe and microscope, samples 1–4 (see table 1) exhibited nacreous surfaces, with fine overlapping platelets visible under high magnification. Surface wrinkling was also seen in single areas on samples 1 and 3, along with fine surface fractures; the wrinkled feature in each was previously noted as a characteristic of a FW environment (Strack, 2015, 2018). The nacreous samples ranged from 0.70 to 2.68 ct and measured from 4.77 × 4.33 mm to 7.08 × 6.72 mm. According to GIA classification procedures, their shapes were semi-baroque, baroque, and circled oval, while their bodycolors varied from light pinkish brown to light purplish pink and very light pinkish brown. Sample 3 showed a dull surface lacking luster and overtone, while the other three displayed orient and pink overtones.

Conversely, samples 5–8 exhibited a non-nacreous surface appearance and lacked overlapping platelets characteristic of most FW pearls. They ranged from 0.94 to 2.11 ct and measured from 5.12 mm to 7.32 × 6.98 mm. The shapes were uniformly round, oval, and drop, and all the samples were brown-yellow. At higher magnification, using strong illumination such as fiber-optic lighting, all the pearls displayed mosaic or cellular surface patterns of differing sizes and shapes. The small cells, which looked like pinpoint features in lower lighting conditions, resulted in a dimpled surface texture (figure 5). A cellular pattern was also observed in a small area on the base of sample 1. The non-nacreous appearance and cellular surface structures resembled those commonly observed on pen pearls from the *Pinnidae* family (N. Sturman et al., "Observations on pearls reportedly from the *Pinnidae* family (pen pearls)," Fall 2014 *G&G*, pp. 202–215), as well as some non-nacreous non-bead cultured pearls from the *Pinctada maxima* mollusk (A. Manustrong et al., "Known non-nacreous non-bead cultured pearls and similar unknown pearls of likely cultured origin from *Pinctada maxima*," *GIA Research News*, 2019, https://www.gia.edu/gia-news-research/known-non-nacreous-non-bead-cultured-pearls). Non-nacreous natural pearls from *Pteria* species mollusks have also reportedly displayed hexagonal-like cellular patterns (S. Karampelas and H. Abdulla, "Black non-nacreous natural pearls from *Pteria* sp.," *Journal of Gemmology*, Vol. 35, No. 7, 2017, pp. 590–592).

Figure 5. At higher magnification, the four non-nacreous pearls displayed mosaic or cellular surface patterns of different sizes and shapes. This image shows the cellular structure on the surface of sample 7 when illuminated with a fiber-optic light. Photomicrograph by Nathan Renfro; field of view 1.00 mm.

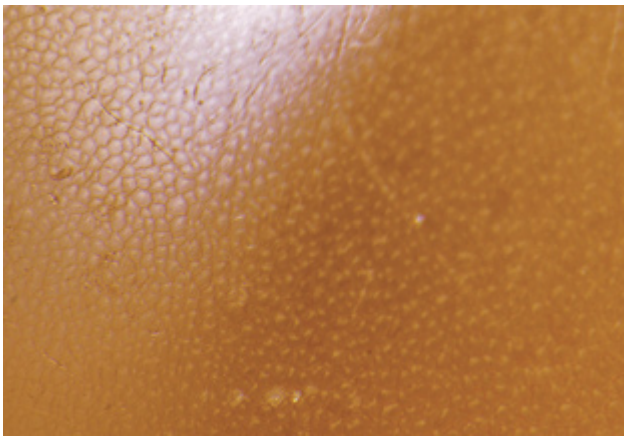

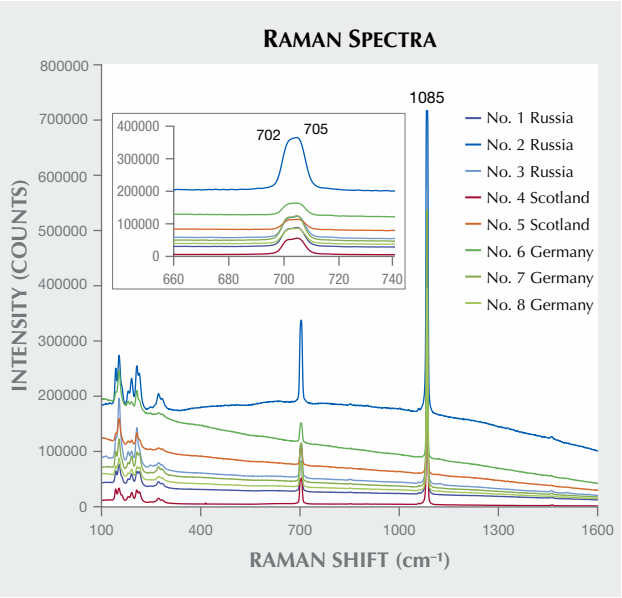

Figure 6. Raman spectra of all eight samples obtained using an 830 nm diode laser revealed clear aragonite peaks, a doublet at 702 and 705 cm^{-1} (magnified in the inset), and a single intense band at 1085 cm^{-1}. These results allowed the four non-nacreous pearls to be separated from pen pearls, which are normally composed of calcite (Sturman et al., 2014). Spectra are offset vertically for clarity.

Under long-wave ultraviolet radiation (365 nm), the nacreous samples exhibited weak bluish yellow fluorescence over most of the surface, while a yellow reaction was observed on the limited yellowish brown areas. The non-nacreous samples exhibited uniform weak to moderate chalky yellow fluorescence similar to that reported for pen pearls (Sturman et al., 2014), but different from the strong orangy red fluorescence observed in non-nacreous *Pteria* pearls (S. Karampelas and H. Abdulla, 2017).

A Raman spectrometer was used to examine the surface composition of all the pearls, initially using a 514 nm argon-ion laser. Owing to the high background fluorescence observed in most of the samples, an 830 nm laser provided better peak resolution. Clear aragonite peaks at 702, 705, and 1085 cm^{-1} were recorded in all the samples (figure 6), and the results allowed the four non-nacreous pearls to be separated from pen pearls, which are normally composed of calcite (Sturman et al., 2014). Raman spectra collected using the 514 nm laser revealed weak polyene peaks at approximately 1125 cm^{-1} and 1512 cm^{-1} in samples 1, 3, and 4, indicating their colors were natural. Polyene peaks were not observed in samples 2 and 5–8, possibly due to the samples' high fluorescence. The 830 nm laser is not helpful in resolving polyenic peaks. Surface observations did not reveal color modification in any of the samples.

UV-Vis reflectance spectra were collected from the smoothest and most homogeneously colored area of each sample in the 250–800 nm range. An absorption feature at about 280 nm that is usually observed in nacreous pearls was clearly seen in samples 1–4 but absent in samples 5–8. Samples 1, 2, and 4 showed reflection minima in the blue to yellow range, which corresponds with their predominantly pink hue. These results correlate with those in a previous study on naturally pink FW pearls of natural origin from the Mississippi River System in the United States (Summer 2019 GNI, pp. 282–285) and with reports on natural-color FW cultured pearls from *Hyriopsis* species mollusks (S. Karampelas et al., "Role of polyenes in the coloration of cultured freshwater pearls," *European Journal of Mineralogy*, Vol. 21, No. 1, 2009, pp. 85–97; A. Abduriyim, "Cultured pearls from Lake Kasumigaura: Production and gemological characteristics," Summer 2018 *G&G*, pp. 166–183). Owing to the very light color of sample 3, the spectrum obtained was nearly flat, as would be expected for white pearls, and hence no features of any significance were observed. The spectra obtained from samples 5–8 showed a lower reflectance than the four previously reported samples due to their more saturated colors. All the spectra showed similar patterns, with an incline from 400 to 750 nm in the visible region, comparable to the reported spectra of dark-colored pen pearls (Sturman et al., 2014) and non-nacreous non-bead cultured pearls from *Pinctada maxima* (Manustrong et al., 2019).

Table 1 shows the internal structures of the eight samples using real-time microradiography (RTX) and X-ray computed microtomography (μ-CT). Sample 1 and all the non-nacreous samples showed clear organic-rich concentric ring structures with faint radial features radiating outward from the center across the concentric rings. The radial structures are associated with cellular surface patterns. All three sections of sample 2 showed weak growth arcs corresponding to their shapes. Sample 3 exhibited a wavy concentric growth pattern together with a dark organic-rich patch, while μ-CT analysis revealed a small dark core in the structure. Sample 4 displayed the least amount of visible structure—only a few very faint growth arcs, even when examined using μ-CT. Cracks of varying lengths and degrees of visibility were present in the samples. The structures observed confirmed their stated natural origin. However, a smaller nucleus with a lighter gray core next to the main nucleus in sample 7 did raise some concerns. If the pearl was submitted to a gemological laboratory without any known provenance, the smaller structure could be mistaken for the lighter gray carbonate "seed" features sometimes found in saltwater non-bead cultured pearls (M.S. Krzemnicki et. al., "Tokki pearls: Additional cultured pearls formed during pearl cultivation: External and internal structures," *32nd International Gemmological Conference*, 2011, https://www.ssef.ch/wp-content/uploads/2018/01/SSEF_Tokki_pearls.pdf). However, the authors are not aware that this type of feature has ever been reported in non-bead cultured pearls from a FW environment.

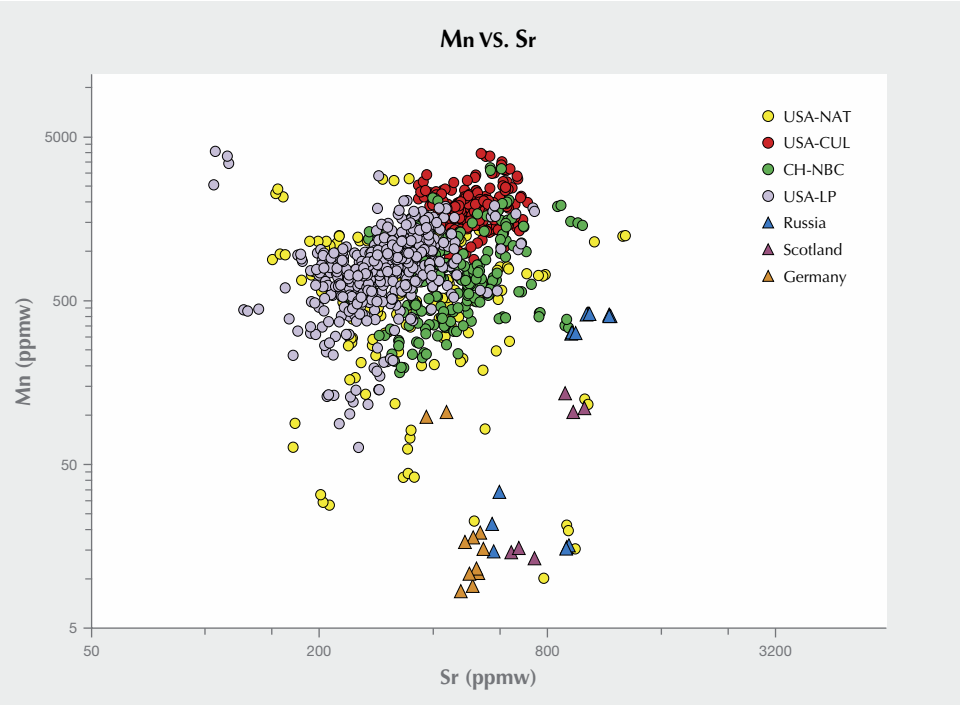

Figure 7. All the European pearl samples contained Mn levels below 500 ppm, which helped separate them from the majority of freshwater pearls previously studied. Mn and Sr levels obtained by LA-ICP-MS analysis were consistent with the EDXRF results. Yellow spots represent results from American natural pearls (USA-NAT), red spots from American cultured pearls (USA-CUL), green spots from Chinese NBC pearls (CH-NBC), and purple spots from American natural pearls from the Mississippi River System (USA-LP).

Chemical compositions were initially analyzed by energy-dispersive X-ray fluorescence (EDXRF) spectrometry, and some of the samples were tested twice in different positions. Most samples contained relatively low manganese (Mn) levels (0 to 240 ppm) compared to the majority of natural and cultured FW pearls in GIA's database. The usual Mn range observed is between 150 and 2000 ppm. Samples 1, 3, and 6–8 showed Mn concentrations below 50 ppm. It was interesting to note that in sample 5, Mn was absent at one end but present (170 ppm) at the opposite end. Additionally, the samples with low Mn levels (<50 ppm) did not show visible reaction under X-ray excitation (H. Hänni et al., "X-ray luminescence, a valuable test in pearl identification," *Journal of Gemmology*, Vol. 29, No. 5/6, 2005, pp. 325–329), as would be expected for such low traces of the element. Strontium (Sr) contents were relatively low (< 1000 ppm) in all the samples, which is characteristic of FW origins. However, the very low concentration of Mn and lack of X-ray fluorescence reactions could create some doubts and lead to some misidentifying them as saltwater (SW) pearls.

Detailed trace element concentrations were analyzed using laser ablation–inductively coupled plasma–mass spectrometry (LA-ICP-MS) with the same parameters used in previous FW pearl studies (A. Homkrajae et al., "Provenance discrimination of freshwater pearls by LA-ICP-MS and linear discriminant analysis (LDA)," Spring 2019 *G&G*, pp. 47–60; Summer 2019 GNI, pp. 282–285). At least three ablation spots were tested on each sample, and the results for the 22 elements selected are shown in table 2. The five elements (sodium, magnesium, Mn, Sr, and barium) found to be useful discriminators in the differentiation of FW from SW pearls and in classifying FW pearls from different sources are bolded in the table. Mn and Sr contents obtained were consistent with the EDXRF results. All the samples contained low Mn levels (<500 ppm), separating them from the majority of FW pearls previously studied (figure 7; see Homkrajae et al., 2019; Summer 2019 GNI, pp. 282–285). The ternary diagram of relative percentages between Ba, Mg, and Mn that was used to verify the growth environment conditions of the questionable FW pearls in previous studies (Homkrajae et al., 2019; Summer 2019 GNI, pp. 282–285) was used once again to confirm the formation environment of the six samples containing low levels of Mn (below 100 ppm). All six samples plotted alongside those of the FW pearls previously studied, confirming their FW origin. These results also help to distinguish non-nacreous samples from saltwater non-nacreous non-bead cultured pearls produced by *Pinctada maxima* (Manustrong et al., 2019). The values of these five discriminant elements, as well as those for lead (Pb), correspond with the chemical results reported on natural FW pearls produced by *Margaritifera margaritifera* mollusks found in the Spey River, Scotland (S. Karampelas et al., "Chemical characteristics of freshwater and saltwater natural and cultured pearls from different bivalves," *Minerals*, Vol. 9, No. 6, 2019, p. 357). The Sr-Ba concentration plot is also shown in figure 8. This result supports the observation made by Karampelas et al. (2019). Furthermore, the pearls from each European locality could be separated from each other in this plot, though it should be noted that this was based on a very limited number of known samples.

For centuries, the freshwater mussel species *Margaritifera margaritifera* was abundant in the rivers and streams

TABLE 2. LA-ICP-MS chemical composition values (in ppmw) of the European pearls studied.

Element	Maximum	Minimum[a]	Average[b]	Detection Limits
Li	1.64	bdl	0.15	0.013
B	98.0	bdl	16.7	0.12
Na	**2300**	**1150**	**1760**	**1.55**
Mg	**1890**	**31.8**	**163**	**0.016**
P	292	8.23	134	0.76
K	475	3.83	78.5	0.11
Ca	404000	389000	395000	24.9
Ti	0.27	bdl	0.27	0.045
Cr	1.82	bdl	0.83	0.13
Mn	**426**	**8.42**	**135**	**0.014**
Fe	209	167	173	0.36
Co	0	bdl	bdl	0.12
Ni	0.78	0.51	0.56	0.022
Cu	24.2	0.87	6.79	0.029
Zn	1.66	bdl	0.37	0.030
Ga	10.1	0.59	3.72	0.039
Sr	**1170**	**382**	**751**	**0.034**
Y	0.037	0	0.004	0
Mo	0.61	bdl	0.061	0.002
Ba	**381**	**22.5**	**147**	**0.009**
La	0.016	0	0.003	0
Pb	0.19	bdl	0.062	0.006

[a]*bdl = below detection limits*
[b]*Data below detection limits is treated as zero when calculating average values*

of Europe, and the pearls produced were part of European culture and history. The American native mussel species followed a similar path. However, environmental changes, and the impact of pollution from industry and agriculture have damaged ecosystems and directly affected the mussels' habitat and lifespan (Strack, 2006). Freshwater pearl fishing in Europe is currently prohibited or under regulation due to the decline of mussel populations. Studying these rare European FW natural pearls provided valuable data that has enlarged GIA's identification database, offering a useful reference for the gemological community.

Artitaya Homkrajae and Ziyin Sun
GIA, Carlsbad
Elisabeth Strack
Hamburg, Germany
Sally Chan Shih
GIA, New York

Unique non-bead cultured freshwater pearls from Lake Biwa, cultured for 14 years. Lake Biwa in Shiga Prefecture has been producing pearls since 1928, when commercial freshwater pearl culturing first started in Japan. Although production decreased in the late twentieth century due to environmental issues and the declining mussel population (S. Akamatsu et al., "The current status of Chinese freshwater cultured pearls," Summer 2001 *G&G*, pp. 97–113), Biwa pearls harvested in the twenty-first century, as well as vintage ones, are popular in the Japanese market. *Hyriopsis schlegelii*, an indigenous freshwater mollusk found in the lake prior to the 1980s, was originally used as the host for pearl culturing before it was replaced by the hybrid *Hyriopsis schlegelii* × *Hyriopsis cumingii* freshwater mollusk.

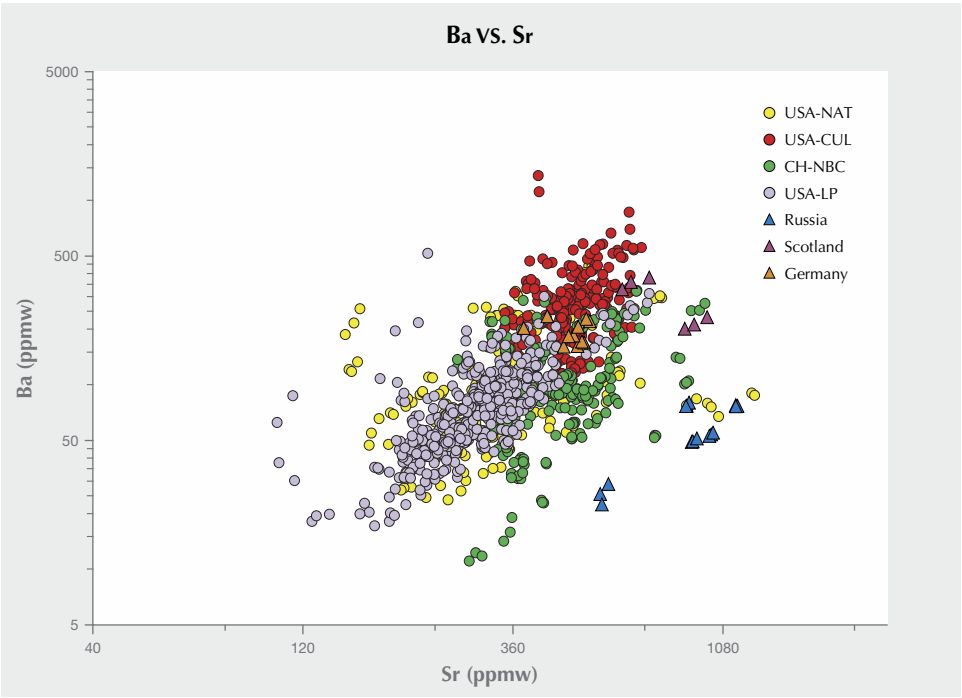

Figure 8. American and Chinese freshwater pearl samples studied previously, together with the samples from this study, were plotted in the Sr-Ba concentration plot. This result supports the observation made by Karampelas et al. (2019). Although the study was based on a limited sample pool, the pearls from each European locality could also be separated using this plot.

Figure 9. The two Biwa pearl samples that were cultured for 14 years and acquired from Jinbo Pearls, measuring 19.75 × 10.38 × 9.84 mm (pearl A, left) and 23.48 × 12.36 × 11.08 mm (pearl B, right). Photo by Shunsuke Nagai.

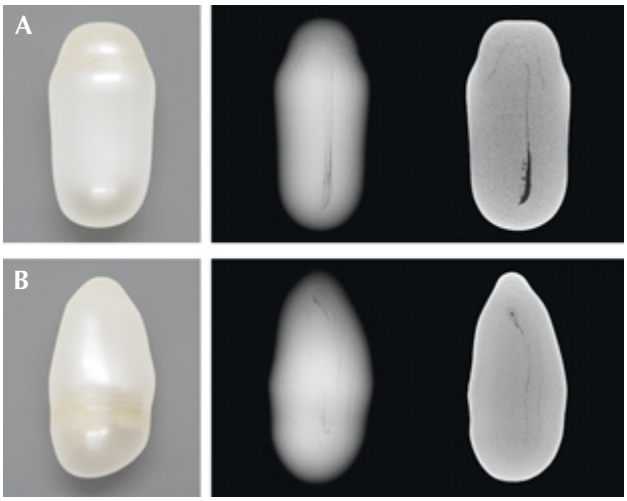

Figure 10. Left: Macro images of pearls A and B. Photos by Nanthaporn Nilpetploy. Center and right: The internal structures as revealed by RTX and µ-CT analysis, respectively.

GIA's Tokyo laboratory received for study 28 pearl samples with a stated Biwa provenance from Jinbo Pearls, a Shiga-based company that deals exclusively with freshwater pearls from Lake Biwa. Two of the largest samples (figure 9), weighing and measuring 16.08 ct, 19.75 × 10.38 × 9.84 mm (pearl A) and 22.85 ct, 23.48 × 12.36 × 11.08 mm (pearl B), respectively (figure 10, left), were selected for further detailed study. The intriguing fact was that they were reportedly grown over a period of 14 years—from 2002 to 2016. This is an unusually long growth period, since freshwater non-bead cultured (NBC) pearls normally take three years to form in Japanese farms. However, the farm where these samples originated was abandoned by the owner due to personal issues. Remarkably, several mussels were found alive when the farm was rechecked before being officially closed by the owner's relatives in 2016. These two pearls were collected from two of the surviving mussels.

Real-time microradiography (RTX) examination revealed a faint linear feature along the length of each pearl (figure 10, center). X-ray computed microtomography (µ-CT) analysis showed these features more clearly and revealed an additional small dark void at the end of pearl A's linear structure (figure 10, right). Their internal structures corresponded well to other non-bead cultured freshwater pearls described in previous studies (M.S. Krzemnicki et al., "X-ray computed microtomography: Distinguishing natural pearls from beaded and non-beaded cultured pearls," Summer 2010 *G&G*, pp. 128–134). Additionally, optical X-ray fluorescence analysis showed a strong yellowish green reaction with weak yellowish orange areas within some imperfections around the circumference of the pearls (indicated by white arrows, figure 11, A-2 and B-2).

Each pearl was cut in half (cut surfaces were cleaned with isopropyl alcohol) and the examination results were compared with those obtained prior to sawing. Surprisingly, both showed stronger reddish orange optical X-ray fluorescence reactions within small areas along the central structure lines (RTX and µ-CT analysis) visible on each sawn face (figure 11, A-4 and B-4) than on any external surface areas when the pearls were intact. Such reactions are sometimes seen in natural and freshwater cultured pearls (Summer 2013 Lab Notes, pp. 113–114; Spring 2019 Lab Notes, pp. 94–96; S. Karampelas et al., "Chemical characteristics of freshwater and saltwater natural and cultured pearls from different bivalves," *Minerals*, Vol. 9, No. 6, 2019, article no. 357, pp. 16–17). It was especially interesting that the reactions seemed to correlate with the dull frosty white surface areas along the central structure lines on the sawn-faces when observed under the microscope at higher magnifications (indicated by black arrows in figure 12, A-3 and B-3). This observation was consistent with previous studies on freshwater cultured pearls (Spring 2019 Lab Notes, pp. 94–96).

Raman analysis of these areas showed they consisted of two $CaCO_3$ polymorphs: aragonite and vaterite. Aragonite features were visible at 701, 704, and 1085 cm^{-1}, while vaterite features were noted at 740, 750, 1075, and 1090 cm^{-1}. Aragonite and vaterite in cultured FW pearls have previously been recorded (U. Wehrmeister et al., "Vaterite in freshwater cultured pearls from China and Japan," *Journal of Gemmology*, Vol. 30, No. 7/8, 2007, pp. 399–412; A.L. Soldati et al., "Structural characterization and chemical composition of aragonite and vaterite in freshwater cultured pearls," *Mineralogical Magazine*, Vol. 72, No. 2, 2008, pp. 579–592; H. Ma et al., "Vaterite or aragonite observed in the prismatic layer of freshwater-cultured pearls from South China," *Progress in Natural Science*, Vol. 19, No. 7, 2009, pp. 817–820). Furthermore, calcite was also detected in pearl A, where peaks at 280, 714, and 1085 cm^{-1} were observed. The first two peaks were isolated and did not appear in association with any other peaks (groupings

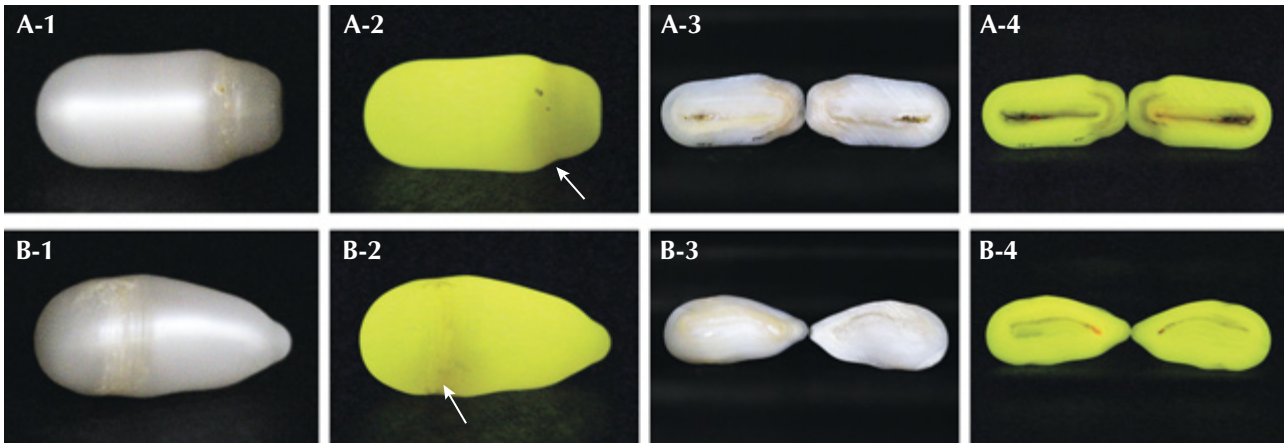

Figure 11. The fluorescence reactions of both pearl samples under optical X-ray fluorescence. The pearls prior to sawing (A-1, B-1) showed strong yellowish green reactions, with some weak yellowish orange areas within some imperfections around their circumference (white arrows, A-2, B-2). The sawn pearls (A-3, B-3) showed strong yellowish green reactions, with stronger reddish orange areas in some positions (A-4, B-4). Images by Kwanreun Lawanwong.

or doublets), proving they were another $CaCO_3$ polymorph. Up until recently, calcite had not been reported in freshwater cultured pearls, though it was found in a small area of pearl A in this study and was also noted in a pearl discussed in a recent study (S. Eaton-Magaña et al., "Raman and photoluminescence mapping of gem materials," *Minerals*, Vol. 11, No. 2, 2021, article no. 177, pp. 24–27).

Further advanced analysis of the cross sections' trace element concentrations was conducted using laser ablation–inductively coupled plasma–mass spectrometry (LA-ICP-MS). The reddish orange fluorescent areas were shown to contain much higher Mg (1250 ppmw for pearl A and 2260 ppmw for pearl B) and lower Na (1210 ppmw for pearl A and 1310 ppmw for pearl B) concentrations than other areas of the samples not exhibiting the reaction (Mg lower than 77 ppmw and Na higher than 1930 ppmw). This result is consistent with those detailed in the literature (Soldati et al., 2008; Eaton-Magaña et al., 2021). The results seemed to correspond with the Raman data, and the different Mg and Na ratios helped to separate aragonite and vaterite, though it is difficult to differentiate calcite from either without performing Raman analysis.

Figure 12. Photomicrographs of the cross sections showing some dull white frosty surfaces (black arrows, A-3, B-3) that correspond to the areas showing reddish orange fluorescent reactions under optical X-ray fluorescence. Field of view 19.20 mm (A-1, B-1), 14.40 mm (A-2, B-2), and 2.88 mm (A-3, B-3). Photos by Kwanreun Lawanwong.

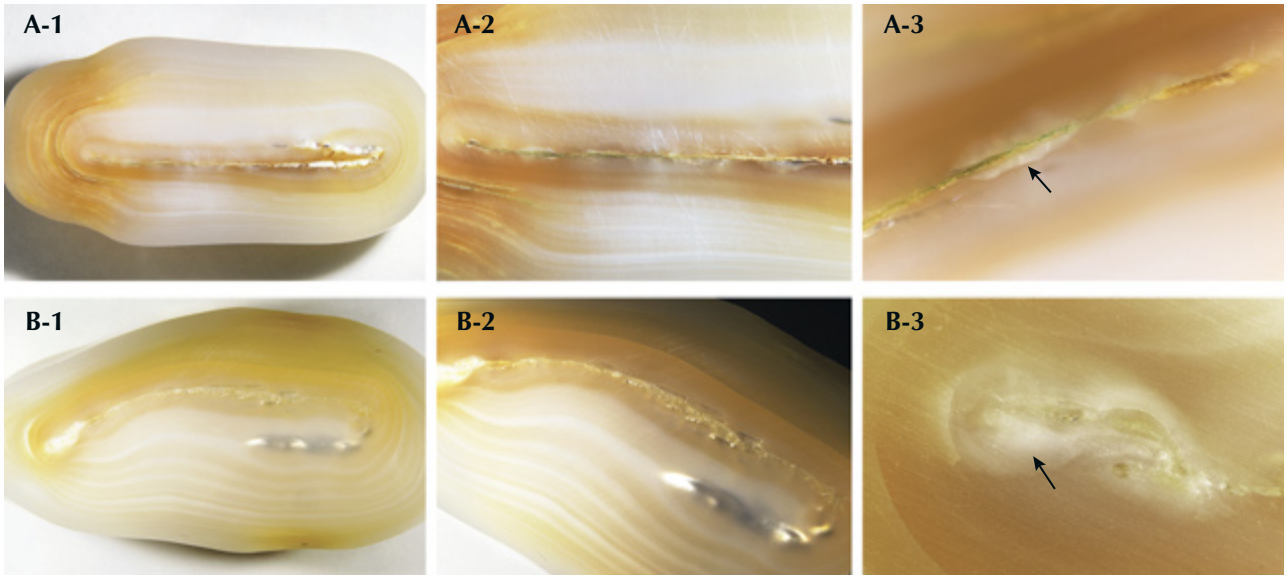

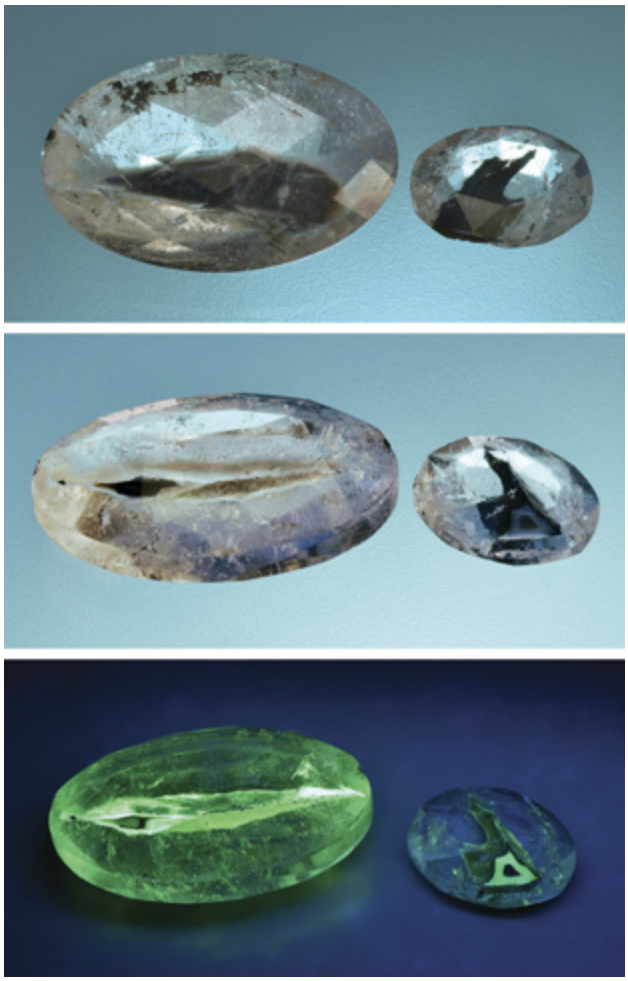

Figure 13. Two faceted quartz with agate inclusions from Brazil, weighing 66.61 ct and 12.28 ct (shown in two positions and in short-wave UV). Photos by Jaroslav Hyršl.

Vaterite within the structure of NBC FW pearls is thought to be related to the biomineralization process that results following the tissue/mantle insertion (Wehrmeister et al., 2007), and its presence is a strong indicator of a cultured origin. These two unique pearls are a part of 28 Biwa pearl samples collected over various time frames. Since they are worthy of being singled out for discussion, this brief report is a precursor to a more detailed review of both pearls and the other Biwa pearl samples referenced.

Nanthaporn Nilpetploy
GIA, Bangkok

Yusuke Katsurada
GIA, Tokyo

Agate inclusion in quartz from Brazil. Agates are undoubtedly one of the most common precious stones from Brazil. They come from basalts in the state of Rio Grande do Sul, on the border with Uruguay. This region is probably also the source of several unusual faceted quartz samples, purchased by the author in Brazil in 2019. These stones are up to 35 mm long and, except for abundant two-phase inclusions, contain flat, irregularly shaped inclusions. On two stones (figure 13), these inclusions reach the surface and show a typical agate structure, with several black, gray, and light brown layers. Their identity was proved by very weak quartz peaks in the Raman spectrum. Unexpected was their strong fluorescence in UV light, which is much stronger in short-wave UV. This fluorescence is concentrated in gray layers and is very likely caused by a trace presence of uranium, quite common in many agates and opals.

Jaroslav Hyršl (hyrsl@hotmail.com)
Prague

Mobile inclusions in a decorative quartz object. A client recently submitted an interesting transparent, highly polished, barrel-shaped object for identification. It weighed approximately 109.2 g, measured approximately 90 × 37 × 22 mm, and clearly exhibited a long brown internal feature (figure 14) containing multi-phase inclusions along the length of the predominantly colorless body. Standard gemological testing resulted in an RI reading of 1.55 (spot) and SG value of 2.61. Microscopic examination revealed fluid, fingerprint, and crystal inclusions typical of a natural growth environment. As a result, the object was identified as natural quartz, which was confirmed by FTIR and Raman analysis.

However, the most notable feature of this specimen was its unique and impressive mobile inclusion scene. On first impression, the long brown inclusion appeared to be a crystal, but it turned out to be a negative crystal filled with countless tiny mobile brownish particles (figure 15) and a large colorless mobile gas bubble. The mobility of these in-

Figure 14. A partial view of the long irregularly shaped brown negative crystal running along the length of its quartz host. Photomicrograph by Lai Tai-An Gem Lab; field of view 6.42 mm.

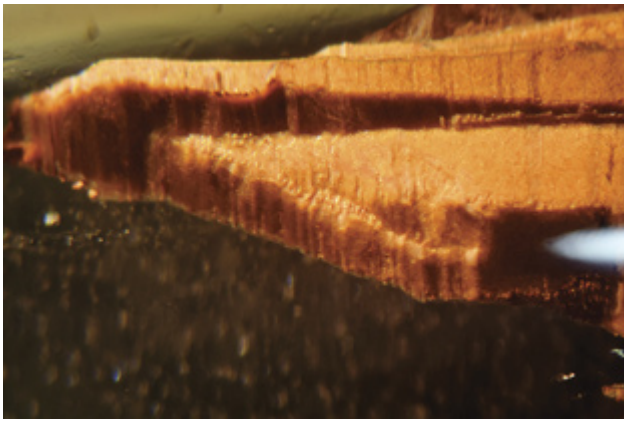

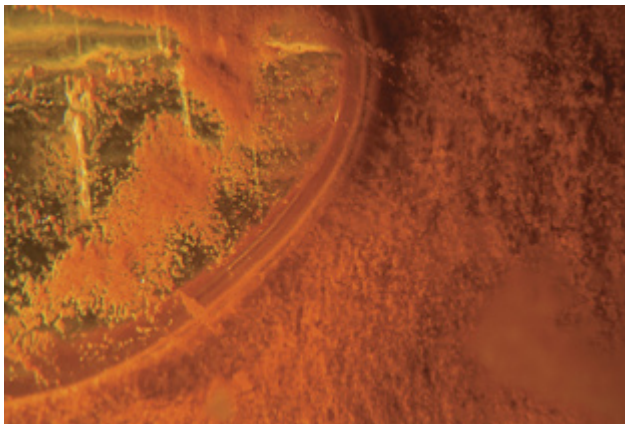

Figure 15. The countless tiny brown particles together with part of the large colorless bubble within the negative crystal. Photomicrograph by Lai Tai-An Gem Lab; field of view 4.57 mm.

clusions within the brown negative crystal was cleverly incorporated into the final design, as the lapidary fashioned the object into a barrel form with flat faces at either end. This allowed the object to be flipped over like an hourglass, so that all the mobile inclusions would be set in motion (figure 16; see video at https://www.gia.edu/gems-gemology/summer-2021-gemnews-mobile-inclusions-quartz). It was also noted that the gas bubble moved at a faster rate than the tiny particles, which made the object even more captivating. The ambient temperature also appeared to affect the speed at which the inclusions moved—the higher the temperature, the faster the rate.

Although the identification of this quartz specimen was straightforward, it was a pleasure to see the artistry employed in its fashioning that permitted its inclusions to be easily seen to maximum effect.

Larry Tai-An Lai (laitaiangemlab@gmail.com)
Lai Tai-An Gem Laboratory, Taipei

Multi-color sapphires reportedly from the Garba Tula district, Isiolo County, Kenya. The Garba Tula sapphire deposit, located in Isiolo County in central Kenya, is a unique igneous gem-corundum producing area. It is a productive source of blue, green, and yellow sapphires (C. Simonet et al., "The Dusi (Garba Tula) sapphire deposit, Central Kenya–A unique Pan-African corundum-bearing monzonite," *Journal of African Earth Sciences*, Vol. 38, 2004, pp. 401–410). Figure 17 shows the overall color appearance of 28 Garba Tula sapphires recently examined in this study. They were purchased from a reliable dealer at the Tucson gem shows in 2019. It was noticed that their color varied from dark blue to yellow through various shades of blue and green. Some showed strong yellow and blue zoning, while samples with bluish and greenish color banding were also observed. Interestingly, one of the sapphires exhibited a color-change appearance (indicated by the black arrow in figure 17). Windows were polished into the samples in order to study their internal features and collect chemical data. For some samples, windows were polished parallel to the c-axis for spectroscopic measurements.

The studied materials revealed a slightly higher refractive index (1.761–1.773) than typical metamorphic sapphires. The other standard gemological properties were typical of natural corundum. The vast majority of these Garba Tula sapphires (75%) displayed no fluorescence under long-wave UV radiation, while 18% fluoresced red and the remainder showed zoned orange fluorescence (with very weak red fluorescence or none). The fluorescence intensity to long-wave UV of Garba Tula sapphires is generally very weak to weak. However, they were totally inert to short-wave UV light.

The characteristic inclusions observed from these 28 Garba Tula sapphire samples are presented in figure 18. More than 90% were included with irregular brownish needles and platelets identified by Raman as hematite/ilmenite (Y. Katsurada et al., "Golden sheen sapphire and syenite/monzonite–hosted sapphire from Kenya," Fall

Figure 16. A series of images showing the movement of the tiny brown particles and the large bubble in the barrel-shaped object. The denser particles drop toward the bottom and the bubble rises to the top. When flipped over, the process starts again, reminiscent of an hourglass. Photo by Lai Tai-An Gem Lab.

Figure 17. Color-calibrated photos of sapphires (0.602–7.133 ct) reportedly from the Garba Tula area in the Isiolo region of Kenya. The black arrow indicates the color-change sapphire. Photo by Sasithorn Engniwat.

2018 *G&G*, pp. 322–323), formed either as planes along the color banding or as a group or cloud. These multiple twinning planes, commonly associated with parallel and/or intersecting growth tubes, were found in more than 80% of the stones. A few samples contained numerous single and scattered clusters identified by Raman spectroscopy as zircon crystals (figure 18, right), sometimes with fine rutile needles and reflective particle clouds, but with fewer irregular brownish platelets. Fingerprint inclusions as well as the other crystal inclusions identified using Raman spectroscopy and the RRUFF reference database, such as apatite and mica, were occasionally observed in the Garba Tula sapphires studied. Moreover, crystals of carbonate minerals were also previously reported in Garba Tula sapphire (Y. Katsurada et al., 2018). However, they typically lack sharp growth structure and milky clouds, as frequently seen in Madagascar and Sri Lanka.

FTIR spectra obtained from the sapphires often showed one or more diagnostic features: a single 3309 cm^{-1} peak as well as OH-related mineral features such as boehmite,

Figure 18. Typical inclusions presented in the sapphires from Garba Tula, Kenya. Left and center: A plane of irregular reflective needles that showed brownish color using fiber-optic lighting and diffused lighting, respectively; field of view 2.88 mm. Right: Numerous single and clusters of zircon crystals, some with tension fractures; field of view 4.8 mm. Photomicrographs by C. Khowpong and S. Wongchacree.

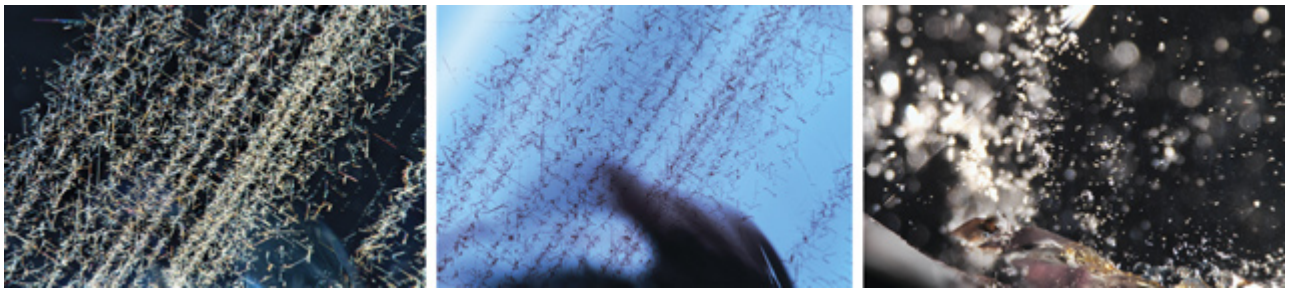

kaolinite, and gibbsite. It was noticed that every sample exhibited a single 3309 cm^{-1} peak without any subordinate peaks, while the boehmite and kaolinite were observed often (>70%) with a small percentage (18%) showing the gibbsite mineral feature.

Interestingly, the UV-Vis-NIR spectrum of greenish blue to blue sapphires from Garba Tula exhibited a metamorphic-type sapphire spectrum, with strong Fe^{3+}-related absorption features at 377, 388, and 450 nm and also an Fe^{2+}-Ti^{4+} intervalence charge transfer (A.C. Palke et al., "Geographic origin determination of blue sapphire," Winter 2019 *G&G*, pp. 536–579). A broad band centered at 880 nm, which is typically used to indicate basalt-hosted sapphire, was not observed.

LA-ICP-MS showed comparable trace element chemistry profiles between the different color areas of the stones, as presented in table 1. The Garba Tula corundum contains significant amounts of Fe and small amounts of Ti. High Fe content ranging from 1555–3177 ppma and 2121–2943 ppma were detected in greenish blue to blue and yellowish to greenish zones, respectively, while the Ti concentration ranged from 3–41 ppma. The high amounts of Fe were also higher than those of Mogok (Myanmar) and Tunduru (Tanzania) sapphires, which have been previously reported as high-Fe metamorphic sources (W. Soonthorntantikul et al., "An in-depth gemological study of blue sapphires from the Baw Mar mine (Mogok, Myanmar)," *GIA Research News*, 2017, https://www.gia.edu/gia-news-research/blue-sapphires-baw-mar-mine-mogok-myanmar). Therefore, the chemical composition of the Garba Tula sapphires, particularly their high Fe, is not common for metamorphic sapphire deposits.

The discovery of this source for yellow, green, and blue sapphires could be interesting for the gem trade. The material represents a true challenge for gemologists working on origin determination, as their formation is quite complicated. Although some properties and chemistry of the Garba Tula sapphires are comparable to the corundum xenocrysts originating from alkali basalt fields, their UV-Vis-NIR and FTIR spectra and their internal features are not consistent with typical basalt-related sapphires. The inclusion scene might, in some aspects, overlap between high-Fe metamorphic and basalt-related sapphires. The reflective/iridescent brownish platelets can be seen in metamorphic sapphires from Mogok, Myanmar, as well as in basalt-hosted sapphires from Thailand and Ethiopia. But none of the glassy melt inclusions usually observed in basalt-related sapphires were noticed in the Garba Tula sapphires. One hypothesis is that they formed in the same way as the basalt-related stones but just were not brought to the surface by the basalt. Therefore, a combination of multiple techniques can be useful in the origin determination of sapphires from Garba Tula.

Ungkhana Atikarnsakul
GIA, Bangkok

DIAMONDS

Rare mixed type IaB-IIb diamond with a long-lasting phosphorescence. Phosphorescence is an optical effect in which electromagnetic radiation absorbed by a substance is released relatively slowly in the form of light. Long-lasting UV phosphorescence of more than 10 seconds' duration is an extremely rare property in natural diamonds, normally limited to hydrogen-rich type Ia chameleon and type IIb diamonds.

Recently, a natural round brilliant weighing 0.20 ct (E-F color, VS_2-SI_1 clarity) was submitted to Stuller Inc. by a client for a custom design. During our diamond screening process, using a phosphorescence imaging-based screening device, the diamond was automatically identified as having an HPHT-grown origin, conflicting with the client's natural origin disclosure. Secondary testing, using a fluorescence spectroscopy-based screening device, identified the diamond as having a natural origin. Under magnification, only a few pinpoints were spotted.

Due to the ambiguous results, the gem was sent to Stuller's Gem Lab for further analysis. The FTIR spectrum (figure 19) showed a mixed diamond type comprising low

TABLE 1. Trace element chemistry of Garba Tula sapphires with different color areas.

Color area		Concentrations (ppma)					
		Mg	Ti	V	Cr	Fe	Ga
Greenish blue to blue	Range	2–29	3–32	0.2–9.0	0.4–55.0	1555–3177	10–85
	Average	7	11	1.6	6.2	2615	36
Yellowish and greenish	Range	2–34	3–41	0.2–8.0	bql[a]–37	2121–2943	12–45
	Average	9	10	2.1	—	2622	32
Detection limits		0.076	0.163	0.012	0.161	1.665	0.008

[a]*bql = below quantification limits*

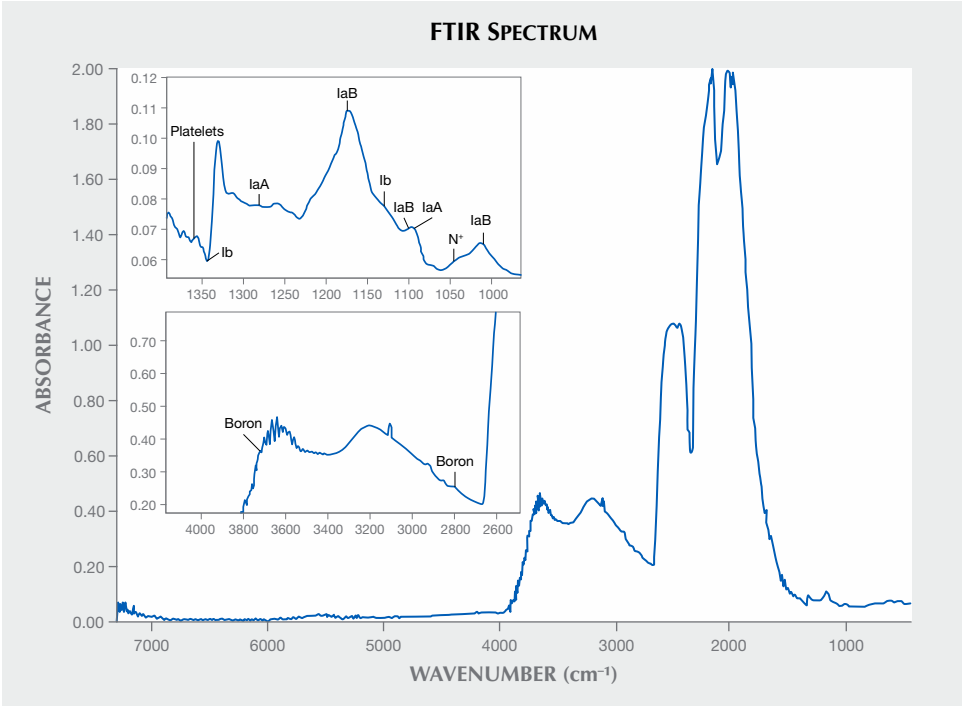

Figure 19. The 0.20 ct diamond's FTIR spectrum. The insets show the type IaB aggregate nitrogen at 1175 and 1010 cm^{-1} (top inset) and IIb boron (bottom inset) at 3725 and 2803 cm^{-1}, confirming a mixed-type stone.

levels of aggregated nitrogen (IaB) and boron (IIb), indicating a natural origin. Similar results were given using fluorescence spectroscopy, which identified N3 peaks, associated with natural origin. Photoluminescence spectroscopy, using a 532 nm laser under liquid nitrogen temperature (77 K), provided results supporting the other instruments and confirming the absence of synthetic origin-related peaks.

In order to identify the cause of the false positive results from the first screening device, the diamond was placed in a SWUV cabinet to analyze its phosphorescence effect. Once excited, the stone emitted a strong bluish green phosphorescence for about 120 seconds (figure 20).

The emitted color and the unusually long duration of the effect are typically associated with HPHT-grown diamonds. Consequently, these properties triggered the false positive results in the phosphorescence imaging-based screening device. In this case, the rare combination of natural diamond types, which includes a boron component, was probably the reason for the unusual phosphorescence.

This case demonstrates the complexity of diamond origin identification and the need for multiple diamond screening devices, each with a different screening technology, to cover all possibilities and ensure a 100% correct identification.

Guy Borenstein and Sean Oneal
Stuller Inc.

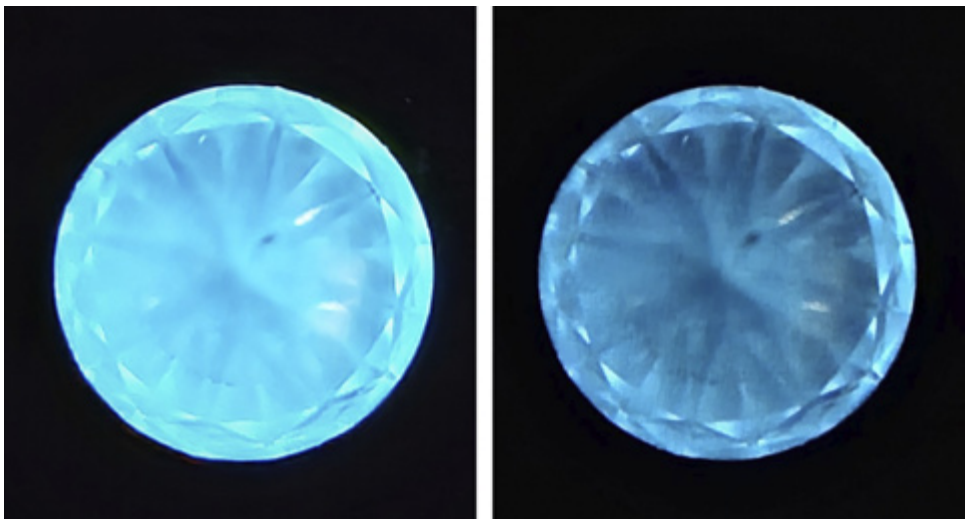

Figure 20. The 0.20 ct diamond's phosphorescence, as seen immediately after exposure to UV radiation (left) and after 60 seconds of elapsed time (right). Images by Guy Borenstein.

SYNTHETICS AND SIMULANTS

Calcareous coral and epoxy composite. Red calcareous coral is very popular in the Taiwanese market and has become far more expensive over the decades due to limited production and increasing demand. Red calcareous coral is usually cut into polished branches, beads, carvings, or cabochons. Recently, a bangle was submitted as calcareous coral to Taiwan Union Lab of Gem Research (TULAB) for identification service. It had a typical coral-red color (figure 21), though it was unusual to see a carved bangle due to the sizes of natural coral specimens that are found.

Standard gemological testing revealed that the refractive indices of this bangle were consistent with calcareous coral, at 1.48–1.65. However, its specific gravity of 2.27 was less than that of calcareous coral (2.6–2.7). Moreover, the short-wave ultraviolet fluorescence of this bangle presented a unique pattern of patches with chalky white to orange fluorescence next to each other (figure 22). Microscopic observations indicated that the patch-like fluorescence seemed to correspond to fragments of red calcareous coral, while the fragments were bonded with red material in which few bubble inclusions were found (figure 23).

To further confirm the identity of this bangle, the patches and the bonding material in between them were analyzed by Raman spectroscopy, and the resulting spectra were then compared with those of epoxy and red calcareous coral reported in the literature (figure 24; see K.E. Chike et al., "Raman and near-infrared studies of an epoxy resin," *Applied Spectroscopy*, Vol. 47, No. 10, 1993, pp. 1631–1635; S. Karampelas et al., "Identification of the endangered pink-to-red *Stylaster* corals by Raman spectroscopy," Spring 2009 *G&G*, pp. 48–52). The results showed that the fluorescing patches were natural calcare-

Figure 21. The carved bangle submitted as "red calcareous coral." Photo by Shu-Hong Lin.

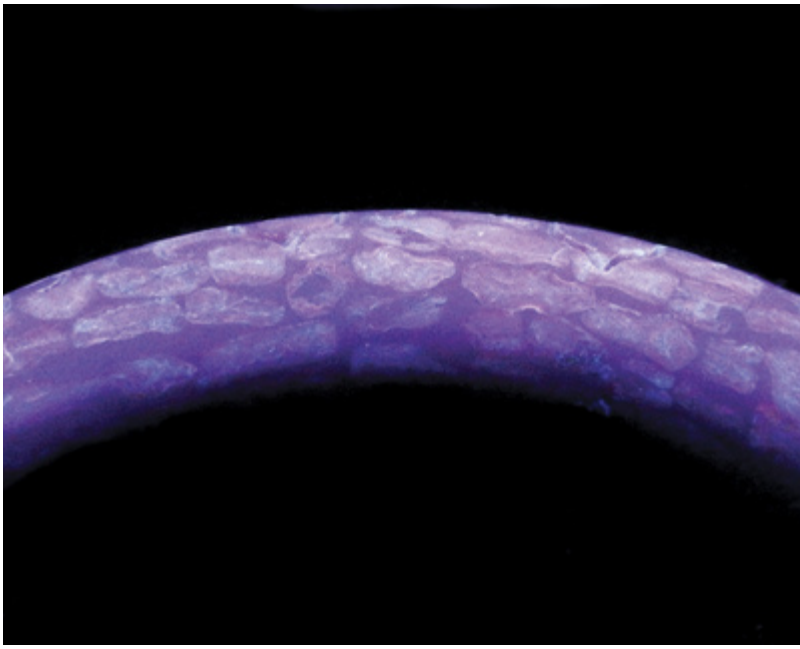

Figure 22. Short-wave ultraviolet fluorescence of the bangle presented a pattern of separate patches fluorescing white to orange. Photo by Kai-Yun Huang.

Figure 23. The microscopic image of the carved bangle indicated that the fluorescing patches seemed to be fragments of red calcareous coral, while the gaps between the fragments were filled with red foreign material with few bubble inclusions. Photomicrograph by Yu-Shan Chou; field of view 5.46 mm.

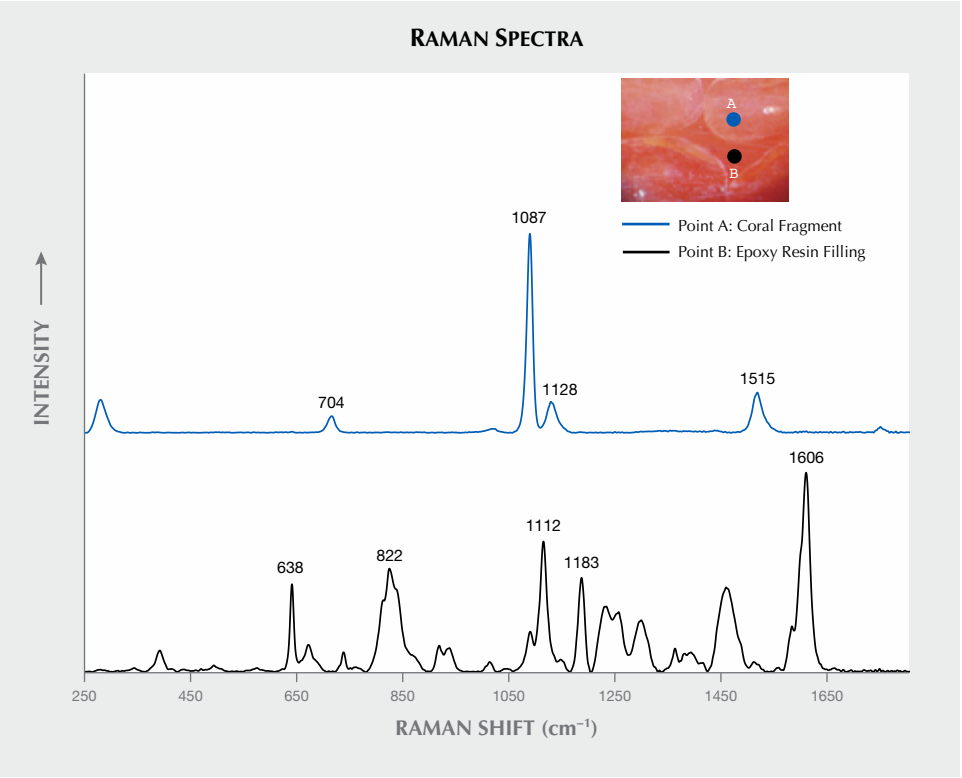

Figure 24. The Raman spectra of the bangle matched those reported in the literature for red calcareous coral and epoxy resin, which meant the bangle was composed of fragments of red calcareous coral (A: Raman peaks at 704, 1087, 1128, and 1515 cm^{-1}) and epoxy filling (B: Raman peaks at 638, 822, 1112, 1183, and 1606 cm^{-1}). The stacked spectra are baseline-corrected and normalized.

ous coral, while the bonding material in between was epoxy resin.

This kind of composite product was likely made by bonding the stacked coral fragments with red epoxy resin to form a bulk material, which was then processed into carvings, cabochons, or even bangles. Although the coral-epoxy composite product looked similar to natural calcareous coral, it could be accurately distinguished through specific gravity, ultraviolet fluorescence reaction, microscopic observation, and Raman spectroscopy.

Shu-Hong Lin
Institute of Earth Sciences, National Taiwan Ocean University
Taiwan Union Lab of Gem Research, Taipei

Kai-Yun Huang
Taiwan Union Lab of Gem Research, Taipei

Yu-Shan Chou
Taiwan Union Lab of Gem Research, Taipei

ANNOUNCEMENTS

Mignone Halls of Gems and Minerals. The American Museum of Natural History in New York City has reopened one of the most beloved spaces for gem enthusiasts with the unveiling of the Allison and Roberto Mignone Halls of Gems and Minerals on June 12, 2021. After a four-year closure, the 11,000-square-foot halls, which house more than 5,000 specimens sourced from 98 countries, have been completely redesigned and reinstalled to tell the intriguing story of how mineral diversity arose on our planet. This exciting public event reflects the reopening of New York City.

The American Museum of Natural History has a long-standing history with minerals and gems that dates back to its founding in 1869. In the 45 years since the previous iteration of the gem and mineral halls opened, the scientific fields of mineralogy and geology have advanced significantly, and the new design reflects these advancements. The halls were organized by Dr. George E. Harlow, curator of the Department of Earth and Planetary Sciences, to showcase to the public the current scientific understanding of gems and minerals, the geological conditions and processes by which they form, and introduce the relatively novel concept of mineral evolution.

Mineral evolution, one of the central themes, seeks to explain how more than 5,500 mineral species came into existence when there were no minerals for hundreds of millions of years after the Big Bang. The new halls show how changing conditions on Earth allowed more chemically diverse minerals to arise. They highlight one of the most important changes, which is the evolution of life that filled the atmosphere with free oxygen, enabling colorful, highly oxidized minerals. These are the same colorful minerals we associate with the gemstones humans have used to decorate themselves for thousands of years.

The redesigned space no longer resembles a simulated subterranean mine, with the multi-leveled carpeted inte-

Figure 25. One of the two giant amethyst geodes displayed at the entrance of the Mineral Hall. This geode weighs 11,000 lbs. (5,000 kg). Photo by Augusto Castillo.

rior that the previous iteration was known for. Instead, an open-floor concept allows visitors to wander seamlessly between the different displays and exhibits. It has three main divisions: the Mineral Hall, the Gem Hall, and the Melissa and Keith Meister Gallery for temporary exhibitions.

Entering the Mineral Hall, the visitor is welcomed by a pair of towering amethyst geodes that formed nearly 135 million years ago (figure 25). The scale and rich purple color of the massive geodes command attention and set the tone for the rest of the space. Behind the geodes, the center of

Figure 26. The Singing Stone is a massive 7,200 lb. (3265 kg) block composed of the copper ore minerals azurite and malachite. Its name comes from the high-pitched sounds produced when the stone absorbed and released moisture from the air. The stone no longer sings now that it sits in a controlled environment. Photo by Augusto Castillo.

the Mineral Hall contains mineral specimens organized by formation environment: igneous, pegmatitic, metamorphic, hydrothermal, and weathering. Highlights include the Singing Stone, a massive block composed of blue azurite and green malachite that was collected in 1891 from Bisbee, Arizona (figure 26), and a 14,500 lb. slab from upstate New York that is studded with garnets measuring up to one foot across (figure 27, opposite page).

The west wall of the Mineral Hall has a running display dedicated to the systematic classification of minerals. The display contains 659 specimens arranged by chemical composition, increasing in complexity across the wall. An interactive periodic table that can be used to explore forming minerals stands at the center of the west wall. The four corners of the Mineral Hall explore the overarching scientific concepts of minerals, from their evolution and diversity to their properties and how they have been used by humans from prehistory to the present day. Adjacent to the gallery of minerals and light is the Gem Hall. It features a dazzling

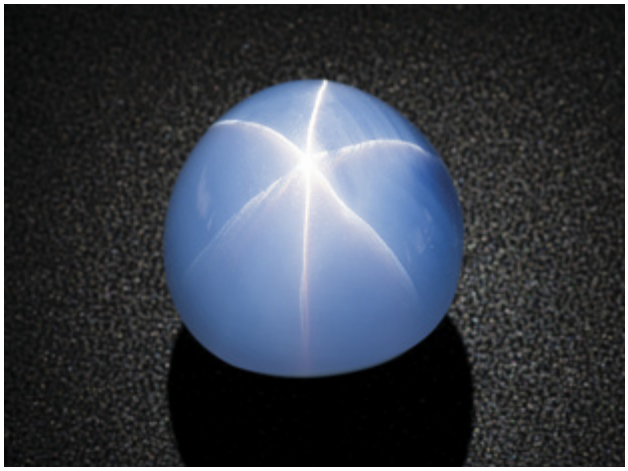

Figure 28. The 563 ct Star of India, the world's largest gem-quality blue star sapphire. Photo by D. Finnin/ ©AMNH.

Figure 27. A towering 14,500 lb. (6,577 kg) slab studded with giant garnets. The garnets formed more than 1 billion years ago, when the original rock transformed at pressure 8,000 times greater than atmospheric pressure and at about 1500°F (815°C). Photo by Augusto Castillo.

Figure 29. The 632 ct Patricia emerald, discovered in 1920 by a local miner, is the largest gem-quality emerald reported from the Chivor mine in Colombia. Photo by D. Finnin/©AMNH.

display of nearly 2,500 objects, including precious stones, carvings, and jewelry from the museum's world-class collection. Highlights include the 563 ct Star of India (figure 28), the largest gem-quality star sapphire known, and the 632 ct Patricia emerald, the largest gem-quality emerald reported from the Chivor mine in Colombia (figure 29).

In addition, the Melissa and Keith Meister Gallery is a rotating exhibit gallery newly added to the Halls of Gems and Minerals. *Beautiful Creatures*, curated by jewelry historian Marion Fasel, features animal-themed jewelry created over the last 150 years. The exhibit included more than 100 jewels from the world's great jewelry houses organized into three categories: land, water, and air. Its time frame coincides with the founding of the American Museum of Natural History in 1869 and explores the extraordinary diversity of the animal kingdom and the inspiration that it has provided for jewelry designers. *Beautiful Creatures* is on display through September 19, 2021.

Augusto Castillo
GIA, New York